

# CyclicFL: A Cyclic Model Pre-Training Approach to Efficient Federated Learning

Pengyu Zhang<sup>1</sup>, Yingbo Zhou<sup>1</sup>, Ming Hu<sup>2</sup>, Xin Fu<sup>3</sup>, Xian Wei<sup>1</sup>, and Mingsong Chen<sup>1\*</sup>

<sup>1</sup>Shanghai Key Lab of Trustworthy Computing, East China Normal University

<sup>2</sup>Nanyang Technological University

<sup>3</sup>University of Houston

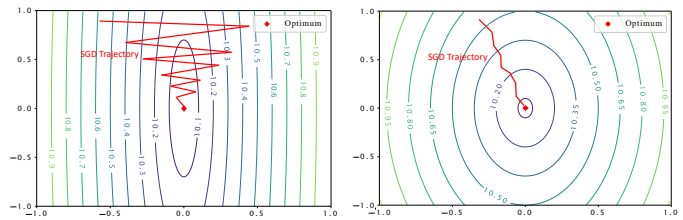
<sup>1\*</sup>Corresponding Author, Email: mschen@sei.ecnu.edu.cn

**Abstract**—Since random initial models in Federated Learning (FL) can easily result in unregulated Stochastic Gradient Descent (SGD) processes, existing FL methods greatly suffer from both slow convergence and poor accuracy, especially for non-IID scenarios. To address this problem, we propose a novel FL method named CyclicFL, which can quickly derive effective initial models to guide the SGD processes, thus improving the overall FL training performance. Based on the concept of Continual Learning (CL), we prove that CyclicFL approximates existing centralized pre-training methods in terms of classification and prediction performance. Meanwhile, we formally analyze the significance of data consistency between the pre-training and training stages of CyclicFL, showing the limited Lipschitzness of loss for the pre-trained models by CyclicFL. Unlike traditional centralized pre-training methods that require public proxy data, CyclicFL pre-trains initial models on selected clients cyclically without exposing their local data. Therefore, they can be easily integrated into any security-critical FL methods. Comprehensive experimental results show that CyclicFL can not only improve the classification accuracy by up to 16.21%, but also significantly accelerate the overall FL training processes.

## I. INTRODUCTION

As a vital decentralized learning paradigm, Federated Learning (FL) is promising to facilitate cloud-client collaboration applications, e.g., Artificial Intelligence of Things (AIoT) [36], Finance Fraud Detection [35], and Brain Tumor Segmentation [31]. To avoid disclosure of privacy, in each FL communication round, all the involved clients firstly conduct local training and then upload their local gradients rather than private data to the cloud. The server updates the global model by aggregating received local gradients and dispatches the updated global model to clients for a new round of training. In this way, the clients can share their knowledge while their data privacy can be safely guaranteed.

Although FL is becoming increasingly popular in the design of security-critical applications, it suffers from slow convergence and poor accuracy, especially in non-IID (Independent and Identically Distributed) scenarios [39]. This is mainly because the inconsistencies of statistical properties among client data inevitably lead to learning divergences during the training of local models [33], which strongly degrade the performance of global model aggregation. Things become even worse when the initial client models are initialized randomly within a non-IID scenario. In this case, since clients incline



(a) A slow SGD process with notable divergences caused by a random initial model. (b) Quick convergence of an SGD process under the guidance of some pre-trained model.

Fig. 1: A motivating example showing the importance of pre-training for FL. (a). With a randomly initialized model, the SGD process suffers from a sharp loss landscape, resulting in slow convergence. (b). Under the guidance of pre-trained models, the SGD process can quickly find the optimum on a flat loss landscape.

to approach their local optimums during the FL training, it is hard for them to reach a consensus [21].

To improve the performance of FL training, various optimization methods have been proposed. Unlike traditional post-processing methods (e.g., knowledge Distillation (KD)-based methods [11]), pre-training methods [5] can implicitly capture transferable consensus in the feature space to further improve FL performance. By establishing a better initialization for model parameters, pre-training is extraordinarily beneficial to downstream tasks by introducing affordable steps of fine-tuning [12]. As an example shown in Figure 1(a), without pre-training, the FL training starts with a randomly initialized model. Here, we can observe an extremely fluctuating Stochastic Gradient Descent (SGD) trajectory to reach an optimal global model. According to [3], the reason for such a detour is mainly due to the sharp loss landscape. Figure 1(b) shows another case, where the FL training starts with a pre-trained model. Since pre-training can create a flatter loss landscape to stabilize and accelerate the downstream training [23], we can find that the SGD trajectory in Figure 1(b) is way more stable, indicating a better FL training performance.

Although pre-training can substantially benefit the FL training, existing pre-training methods assume the existence of numerous proxy data, which is not true in practice. Worse still, even if such proxy data is available, it is still difficult to infer the data distributions of clients from proxy data, thus restricting the application of pre-training in non-IID scenarios.

Unlike traditional pre-training schemes, in this paper, we propose a novel pre-training method named CyclicFL, which enables quick generation of an effective initial model to accelerate the overall FL training process. Instead of using proxy data, CyclicFL pre-trains initial models using the local data of cyclically selected clients without exposing their local data. Meanwhile, due to the significance of data consistency between the pre-training and training stages of CyclicFL, the benefits of pre-trained models by CyclicFL on SGD processes can be guaranteed. In summary, this paper makes the following three major contributions:

- We propose a novel cyclic pre-training approach that can quickly derive initial models without using proxy data. By guiding the SGD processes on flat loss landscapes, the overall FL training performance can be improved.
- Based on the concept of Continual Learning (CL), we prove that CyclicFL can approximate existing centralized pre-training methods, and formally analyze the significance of data consistency between the pre-training and training stages of CyclicFL.
- We implement CyclicFL on top of both classic and state-of-the-art FL methods, and conduct comprehensive experiments on well-known benchmarks to show the effectiveness of pre-training made by CyclicFL.

## II. RELATED WORK

**Neural Network Initialization.** As neural networks go deeper [32], the initialization of network parameters becomes important to prevent gradients from vanishing or explosion during the training procedure. So far, various initialization methods have been proposed. Xavier-Initialization [8] normalized initial parameters to ensure the same variances of inputs and outputs. Since the Xavier-Initialization is only useful on saturating activation functions such as Sigmoid and Tanh [28], it was further extended to He-Initialization [9], where ReLU [26], a broadly used non-saturating activation function, was taken into consideration. [14] further provided theoretical proof that initializing model parameters with orthogonal groups accelerates convergence compared to that with Gaussian groups. To adapt to more complex architectures used in vision tasks, e.g., ResNet [10], MobileNet [13], [24] proposed an initialization method from the perspective of training dynamics by estimating mutual information between two consecutive layers. [38] proposed a “learning to initialize” scheme by formulating initialization on neural networks as an optimization problem.

**Pre-training in Federated Learning.** Recent work has paid attention to the impact of pre-training in FL. [27] implemented comprehensive experiments and showed that starting federated training from pre-trained models not only improves the overall performances in FL, but also alleviates the notorious local drift problems caused by data heterogeneity. Another work [3] emphasized that pre-trained models can boost model performances and close the gap to centralized training as it makes model aggregation more stable. Furthermore, fine-tuning methods specifically designed for vision-language [29]

and vision [6] tasks were proposed by [4] to explore the benefits of using a pre-trained global model under the FL paradigm. The aforementioned works mainly concentrate on analyzing the impacts of pre-training on FL. Few of them provide solutions on obtaining a pre-trained model for neural networks given task-specific [3] data or on which fine-tuning methods can induce more successful transfers from the pre-trained model to downstream FL tasks [4]. Most of the above methods leverage existing pre-trained models without proposing novel pre-training methods. Our solution, instead, aims to leverage task-specific data and provide a novel pre-training method to improve vanilla FL.

## III. METHODOLOGY

### A. Preliminaries

The goal of a general FL is to jointly learn a shared global model parameterized by  $\mathbf{w}$  while keeping local data private. Considering  $m$  participants with private Non-IID dataset denoted as  $\mathcal{D}_m = \{(\mathbf{x}_{m,j}, y_{m,j})\}_{j=1}^{N_m}$ , we seek to solve the problem below:

$$\min_{\mathbf{w}} f(\mathbf{w}) = \sum_{i=1}^m \frac{N_i}{N} L_i(\mathbf{w}; \mathcal{D}_i), \quad (1)$$

$$\text{where } L_i(\mathbf{w}; \mathcal{D}_i) = \frac{1}{N_i} \sum_{j=1}^{N_i} \ell(\mathbf{w}; (\mathbf{x}_{i,j}, y_{i,j})). \quad (2)$$

Here,  $m$  is the number of clients participating in local training in each round,  $N_i$  denotes the number of instances on client  $i$ , and  $N$  represents the total number of instances.  $L_i(\mathbf{w}; \mathcal{D}_i)$  is the empirical loss on local dataset  $\mathcal{D}_i$  consists of the loss function  $\ell(\cdot)$ . The neural network parameter  $\mathbf{w}$  is assumed to be identical across local clients and the server under a homogeneous architecture setting.

### B. Our Proposed CyclicFL

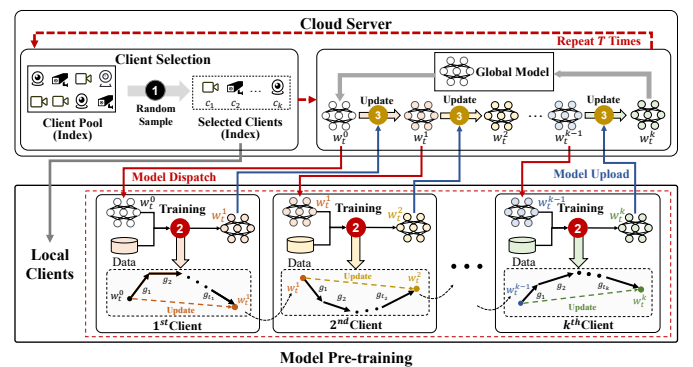


Fig. 2: Workflow of our model pre-training approach

Figure 2 shows the main workflow of our cyclic training method. The entire workflow is built on two alternate steps, i.e., the selection of a group of local participants and the local training. We denote every two consecutive steps as one round. The server on the cloud first performs a group selection step by randomly sampling a group of local participants, on which a series of local training will be conducted. In the meanwhile,

the server creates the randomly initialized model. Note that the server only randomly initializes the model at the beginning of the first round. For simplicity, we use P1 and P2 to denote the cyclic training phase and FL training phase.

---

**Algorithm 1:** Our Cyclic Training Algorithm

---

**Input:**

- i)  $\mathbf{w}_{\text{rg}}$ , a randomly initialized global model;
- ii)  $S$ , a pool of all participants;
- iii)  $T$ , # of cyclic training rounds;
- iv)  $\mathcal{K}_{P1}$ , # of participants in each round.

**Output:**

- i)  $\mathbf{w}_{\text{wg}}$ , a well-initialized global model.

```

1  $\mathbf{w}_1^{1,0} \leftarrow \mathbf{w}_{\text{rg}}$ 
2 for  $t = 1, \dots, T$  do
3    $S_t \leftarrow \text{RandomSample}(S, \mathcal{K}_{P1})$ 
4    $k \leftarrow \text{Number of elements in } S_t$ 
5   for  $i = 1, \dots, k$  do
6     for  $j = 1, \dots, t_i$  do
7        $\mathbf{w}_t^{i,j} = \mathbf{w}_t^{i,j-1} - \mathbf{g}_j$ 
8     end
9      $\mathbf{w}_t^{(i+1),0} \leftarrow \mathbf{w}_t^{i,t_i}$ 
10  end
11   $\mathbf{w}_{t+1}^{1,0} \leftarrow \mathbf{w}_t^{k,t_k}$ 
12 end
13  $\mathbf{w}_{\text{wg}} \leftarrow \mathbf{w}_T^{k,t_k}$ 
14 return  $\mathbf{w}_{\text{wg}}$ 

```

---

Algorithm 1 describes the implementation of cyclic training. At the beginning of cyclic training (Line 1), the cloud server randomly initializes a model parameterized by  $\mathbf{w}_{\text{rg}}$ . Lines 2 – 12 implement  $T$  rounds of cyclic training in total. Line 3 describes a *RandomSample* process, where the cloud server randomly samples a set ( $S_t$ ) of local clients to participate in the local training in this round. In line 4, the constant  $\mathcal{K}_{P1}$  represents the number of clients in set  $S_t$ . After the sampling of local clients is completed, Lines 5 – 10 describe the process of local training. Line 5 represents the outer loop, in which the cloud server broadcasts the global model to the  $i^{\text{th}}$  client to perform the local training. Lines 6 – 8 represent the inner loop, where the  $i^{\text{th}}$  client performs  $t_i$  local training steps (i.e.,  $\mathbf{g}_1, \dots, \mathbf{g}_{t_i}$ ) with its private data. At the end of each inner loop, the local participant sends the trained model back to the server. The server further transmits the trained model to the 1<sup>st</sup> participant in the next round to initiate a new outer loop. Such server-to-local and local-to-server alternate steps are described in Line 9. Line 11 shows the procedure that initiates a new round of cyclic training. Line 13 returns a pre-trained global model parameterized by  $\mathbf{w}_{\text{wg}}$ .

For the notation  $\mathbf{w}_t^{i,j}$ , we use  $t, i, j$  to represent model parameters in the  $j^{\text{th}}$  training step, the  $i^{\text{th}}$  local client, and the  $t^{\text{th}}$  round, respectively. We consider training a neural network parameterized by  $\mathbf{w}_t^0$  on a set of data denoted by  $S_t$  in the  $t^{\text{th}}$  round where  $S_t = \{D_1^t, D_2^t, \dots, D_k^t\}$ . In round  $t$ ,  $k$  datasets that are used to train the model are listed in a fixed order,

i.e., from  $D_1^t$  to  $D_k^t$ , yielding an evolution of neural network parameters from  $\mathbf{w}_t^0$  to  $\mathbf{w}_t^k$ . At the  $i^{\text{th}}$  local client in the  $t^{\text{th}}$  round,  $\mathbf{w}_t^i$  is obtained by fitting model  $\mathbf{w}_t^{i-1}$  on dataset  $D_i^t$  with  $t_i$  steps of optimizations (SGD). The cyclic training is formulated as follows:

$$\min_{\mathbf{w}} \mathcal{F}(\mathbf{w}) = \sum_{t=1}^T \sum_{j=1}^k \ell(\mathbf{w}; D_j^t(n)), \quad (3)$$

where  $\mathcal{F}(\mathbf{w})$  is the objective function of cyclic training, and  $T$  represents the number of rounds cyclic training consumes. Local data of the  $j^{\text{th}}$  client in the  $t^{\text{th}}$  round is denoted as  $D_j^t(n) = \{(\mathbf{x}_{i,1}, y_{i,1}), (\mathbf{x}_{i,2}, y_{i,2}), \dots, (\mathbf{x}_{j,n}, y_{j,n})\}$ . The loss function  $\ell$  is determined by specific tasks, e.g., cross-entropy loss for multi-classification tasks.

Unlike conventional FL algorithms, which directly modify training schemes in FL, our method is completed before arbitrary federated training begins. In conventional FL, the local training aims to search and converge to its optimum, resulting in a local model drift problem. The aggregation process on the server helps to mitigate the local drift problem but cannot completely solve it. The cyclic training, instead, is an attempt to approximate centralized training and enable the global model to converge to one same loss basin [3] from the very beginning. As cyclic training implicitly contains the order of data used to train the neural network, unlike real centralized training, where data are randomly shuffled and packed into batches to have unbiased estimations of the entire dataset, it naturally follows the definition of Continual Learning (CL). As a result, we analyze our method from the angle of CL and explain why cyclic training can approximate centralized training in the next subsection. We also show a plain random selection of clients is adequate to support the success of cyclic training.

### C. Theoretical Analysis

**Approximation to centralized pre-training.** Orthogonal Gradient Descent (OGD) has been proven to be effective in alleviating catastrophic forgetting [1], whereas Stochastic Gradient Descent (SGD) is unable to preserve the knowledge of previous tasks. Therefore, OGD-based training can be naturally treated as centralized training with acceptable knowledge forgetting. However, OGD is not always available in the context of FL. The reasons are from two perspectives: i) OGD requires extra memory to store all gradients on previous datasets. The memory will continuously grow as training goes on and will cause unaffordable storage resource requirements on local clients; ii) Gradient sharing breaks data privacy since data information can be directly recovered from gradients according to [37]. As a result, we seek an alternative scheme, SGD, to replace OGD by considering the characteristics of FL. We provide the theoretical difference between SGD-based and OGD-based training on a sequence of tasks based on Lemma 1 [1] in Corollary 1. We show that the SGD-based method under scenarios of data distribution overlaps approximates OGD, leading to approximating centralized training.

**Lemma 1 (Empirical losses using OGD and SGD).** To simplify mathematical notations, we let  $R_\lambda^\tau$  denote the term  $\frac{\lambda^2}{n_\tau} \tilde{\mathbf{y}}_\tau^\top (\kappa_\tau (\mathbf{X}_\tau, \mathbf{X}_\tau) + \lambda \mathbf{I})^{-1} \tilde{\mathbf{y}}_\tau$ ,  $C$  denotes the constant term  $3c\sqrt{\frac{\log(2/\delta)}{2n_T}}$ , and  $H^\tau$  denotes  $\frac{1}{n_T} \sum_{k=\tau+1}^T H_{k,\tau}$ . The loss function can be rewritten as:

$$\mathcal{L}_{D_\tau}(f_T^*) \leq \begin{cases} R_\lambda^\tau + R_T + C & \text{for OGD, } \tau \in [1, T] \\ R_\lambda^\tau + R_T + C & \text{for SGD, } \tau < T \\ R_\lambda^\tau + H^\tau + R_T + C & \text{for SGD, } \tau = T. \end{cases} \quad (4)$$

**Corollary 1 (The difference between SGD and OGD).** Let  $n_T$  be the number of training samples in task  $T$ . The model acquired by fitting tasks up to  $T$  is represented by  $f_T^*$ . The difference is formulated as follows:

$$\begin{aligned} \text{Diff} &\triangleq \sum_{\tau=1}^T \mathcal{L}_{D_\tau}^{\text{SGD}}(f_T^*) - \mathcal{L}_{D_\tau}^{\text{OGD}}(f_T^*) \\ &\leq R_T + \frac{1}{n_T} \sum_{\tau=1}^{T-1} \sum_{k=\tau+1}^T H_{k,\tau}. \end{aligned} \quad (5)$$

In Corollary 1,  $\text{Diff}$  is greater than 0 since the upper bound of SGD is larger than that of OGD.  $\mathcal{L}_{D_\tau}^{\text{SGD}}(\cdot)$  represents the loss on dataset  $D_\tau$  given the model trained by SGD.  $\mathcal{L}_{D_\tau}^{\text{OGD}}(\cdot)$  instead represents the loss on  $D_\tau$  given the model trained by OGD. The difference in the loss between SGD and OGD is upper bounded by the summation of residual term  $\frac{1}{n_T} \sum_{\tau=1}^{T-1} \sum_{k=\tau+1}^T H_{k,\tau}$  and the task similarity term  $R_T$ . More explanations on  $H_{k,\tau}$  and  $R_T$  are presented in Appendix A. Note that both  $H_{k,\tau}$  and  $R_T$  decrease as task similarity increases. Since both  $H_{k,\tau}$  and  $R_T$  relate to task similarity, we can obtain a tighter upper bound if the task similarity increases. Such an increase shows that SGD-based optimization is closer to OGD-based optimization, therefore, closer to centralized training. In practical FL scenarios, the server doesn't know about the data distributions of local clients due to privacy concerns. The overlap of data distributions across local clients is another practical scenario, where the FL environment consists of massive clients against a few categories of data, e.g., 100 clients collaboratively train a global model on a 20 classes image classification task. Considering these practical circumstances, we claim that adopting a random sampling of all local clients in each training round can allow high chances of replay on similar datasets. The gap between SGD and OGD in FL settings will be decreased accordingly.

**Data consistency on Lipschitzness of loss.** Corollary 1 provides explanations on the approximation of cyclic training-based pre-training to centralized pre-training. In Lemma 2, we show that the success of pre-training also depends on consistency over the pre-training and FL datasets. In contrast, breaking such consistency directly causes the failure of a pre-training process.

**Lemma 2 (The impact of transferred features on the Lipschitzness of the loss).** Let  $Q$  represent the target dataset and  $P$  represent the pre-training dataset,  $\text{poly}$  represent a polynomial. For a two-layer network with a large number

( $m$ ) of hidden neurons, if  $m \geq \text{poly}(n_P, n_Q, \delta^{-1}, \lambda_P^{-1}, \gamma^{-1})$ ,  $\gamma = O\left(\frac{n_P n_Q^{\frac{1}{2}}}{\lambda_P^2 \delta}\right)$ , with a probability no less than  $1 - \delta$  over the random initialization, the Lipschitzness of loss is formulated as follows:

$$\begin{aligned} \left\| \frac{\partial L(\mathbf{w}(P))}{\partial \mathbf{X}^1} \right\|^2 &= \left\| \frac{\partial L(\mathbf{w}(0))}{\partial \mathbf{X}^1} \right\|^2 - \mathbf{y}_Q^\top \mathbf{y}_Q \\ &+ (\mathbf{y}_Q - \mathbf{y}_{P \rightarrow Q})^\top (\mathbf{y}_Q - \mathbf{y}_{P \rightarrow Q}) \\ &+ \frac{\text{poly}(n_P, n_Q, \delta^{-1}, \lambda_P^{-1}, \gamma^{-1})}{m^{\frac{1}{4}}} \\ &+ O\left(\frac{n_P^2 n_Q^{\frac{1}{2}} \gamma}{\lambda_P^2 \delta}\right), \end{aligned} \quad (6)$$

where  $0 < \gamma \leq 1$  controls the magnitude of initial network parameters  $\mathbf{w}(0)$ , which follows a Gaussian distribution.

Constants  $n_p$  and  $n_Q$  represent the number of training samples in the pre-training and target datasets, respectively. The corresponding labels are denoted as  $\mathbf{y}_p$  and  $\mathbf{y}_Q$ , respectively. The matrix  $\mathbf{X}^1$  denotes the activations of the neural network in the target dataset. The minimum eigenvalue of Gram matrix  $H_P^\infty$  and  $H_Q^\infty$  are represented by  $\lambda_P$  and  $\lambda_Q$ , respectively, which are explained in Appendix A. Note that Lemma 2 directly follows what was defined in [7, 23]. It shows the Lipschitzness of loss is controlled by the similarity between tasks in both input and labels. The Lipschitzness depicts the continuity of a given loss function, which shows the flatness of the loss landscape. If the pre-training label is similar to the target task label, the difference between labels is smaller, leading to a decrease of the term  $\|\mathbf{y}_Q - \mathbf{y}_{P \rightarrow Q}\|_2^2$ , thus increasing the Lipschitzness of the loss function. Combining the theoretical property of loss basins with experimental observations from [3], we conclude that since a flat loss basin helps to stabilize FL, maintaining a high similarity between pre-training data and FL data is necessary.

#### IV. PERFORMANCE EVALUATION

We compared our cyclic training-based pre-training method with random initialization on four representative FL algorithms. Experiments were implemented in four image benchmarks and one text prediction benchmark. Our experiments were implemented on a Ubuntu workstation with an Intel i9-12900K CPU, and an NVIDIA GeForce RTX 3090Ti GPU. To show the advantages of cyclic training, we designed experiments to answer the following four research questions.

**RQ1 (Classification Performance):** What are the advantages of cyclic training across all experiments?

**RQ2 (Convergence Performance):** How does the pre-trained model affect convergence?

**RQ3 (Impact of Cyclic Training Duration):** Considering the trade-off between accuracy and convergence speed, when should we switch from P1 to P2?

**RQ4 (Impact on Loss Landscapes):** How does cyclic training affect the final loss landscape?

TABLE I: Test accuracy comparison results. Since Moon is specifically designed for vision tasks, we do not apply it to Shakespeare.

Model	Dataset	Non-IID Setting ( $\beta$ )	Accuracy (%)					
			FedAvg	FedProx	SCAFFOLD	Moon	Cyclic + FedAvg	
CharLSTM-256	Shakespeare	-	56.34	46.73	56.44	-	<b>57.04</b>	
CNN-FEMNIST	FEMNIST	-	81.44	81.44	<b>83.48</b>	81.46	82.95	
CNN-Fashion-MNIST	Fashion-MNIST	0.1	76.18	76.11	78.50	76.28	<b>83.11</b>	
		0.5	84.02	84.01	85.37	83.94	<b>86.83</b>	
		1.0	86.28	86.18	86.11	85.89	<b>88.46</b>	
LeNet-5	CIFAR-10	0.1	49.05	49.00	<b>53.40</b>	48.90	53.38	
		0.5	53.22	52.88	<b>60.14</b>	52.27	57.91	
		1.0	55.11	55.01	<b>61.40</b>	54.82	57.46	
ResNet-8	CIFAR-100	Coarse	0.1	37.73	38.71	35.83	37.09	<b>53.94</b>
			0.5	54.83	54.72	52.55	54.28	<b>64.46</b>
			1.0	58.07	57.66	55.91	57.63	<b>66.12</b>
		Fine	0.1	40.40	40.80	42.54	41.93	<b>54.27</b>
			0.5	47.65	47.79	48.76	47.76	<b>57.06</b>
			1.0	47.63	48.54	48.75	48.76	<b>56.41</b>

### A. Experimental Settings

**Datasets.** We evaluated the performances of our CyclicFL on four image classification tasks: FEMNIST [2], Fashion-MNIST [34], CIFAR-10, CIFAR-100 [17], and one character prediction task: Shakespeare [2]. Note that each image in CIFAR-100 is tagged with “Coarse Label” and “Fine Label”. We use “C” and “F” to represent “Coarse” and “Fine”, respectively, to fully exploit the data. More details of the four datasets are explained in Appendix B. Following the heterogeneity configurations in [22], we considered Dirichlet distribution throughout this paper. The Dirichlet distribution is parameterized by a coefficient  $\beta$ , denoted as  $Dir(\beta)$ .  $\beta$  determines the degree of data heterogeneity. The smaller the  $\beta$  is, the more heterogeneous the data distributions will be. We established three Non-IID scenarios by setting  $\beta$  as 0.1, 0.5, and 1.0, respectively. Since both FEMNIST and Shakespeare datasets are generated with natural Non-IID settings, we did not apply extra splits.

**Models.** To show the scalability of cyclic training to various types of models, we utilized the LeNet-5 [18], which composes of two convolutional layers followed by three full-connected layers, for the CIFAR-10 dataset, and ResNet-8 [10] with batch normalization, which consists of three basic residual blocks, for CIFAR-100. For FEMNIST, we applied a model consisting of two convolutional layers and one fully-connected layer. A model composed of two convolutional layers followed by a dropout layer and two fully-connected layers are used for Fashion-MNIST. On the Shakespeare dataset, we used the LSTM-256.

**Baselines.** We first conducted cyclic training to obtain a pre-trained model, then utilized FedAvg as the basic FL algorithm to compare to other FL algorithms. We evaluated our method on four representative FL algorithms: FedAvg [25], FedProx [20], SCAFFOLD [16], and Moon [21]. The hyper-parameters configurations are presented in Appendix B.

### B. Results and Analysis

**Classification performance.** Table I shows the top-1 test accuracy for all FL baselines under Non-IID settings. For CIFAR-100-Coarse/Fine dataset, we can observe that Cyclic+FedAvg greatly beat four basic FL algorithms. For CIFAR-100-Coarse with  $\beta = 0.5$ , Cyclic+FedAvg outperforms FedAvg, FedProx, SCAFFOLD, and Moon by 9.63%,

9.74%, 11.91%, and 10.18%, respectively. For CIFAR-10, we can observe that SCAFFOLD consistently outperforms other methods, including Cyclic+FedAvg. Since our method is a pre-training process to initialize the global model, the higher classification accuracy of SCAFFOLD compared to Cyclic+FedAvg is not against the effectiveness of cyclic training.

TABLE II: Comparison of test accuracy improvements

Algorithms	Accuracy (%)	
	w/o Cyclic+	w/ Cyclic+
FedAvg	53.22	<b>57.91(+4.69)</b>
FedProx	52.88	<b>57.72(+4.84)</b>
Moon	52.27	<b>57.89(+5.62)</b>
SCAFFOLD	60.14	<b>60.47(+0.33)</b>

Table II compares the accuracy of Cyclic+Y, where Y represents FL baselines (FedAvg, FedProx, SCAFFOLD, and Moon). We can find that cyclic training is compatible with these representative FL algorithms, and it improves classification accuracy on FedProx, Moon, and SCAFFOLD by 4.84%, 5.62%, and 0.33%, respectively. Figure 3 presents the learning curves of Cyclic+Y experiments. The four FL algorithms are depicted with dash-dotted lines, and their Cyclic+ versions are plotted in solid lines. For the Fashion-MNIST dataset, the cyclic training consistently outperforms all baselines. For FEMNIST, the superior of SCAFFOLD compared to Cyclic+FedAvg has the same reason we explained for CIFAR-10. For Shakespeare, Cyclic+FedAvg improves prediction accuracy against FedAvg, FedProx, and SCAFFOLD by 0.7%, 10.31%, and 0.6%, respectively.

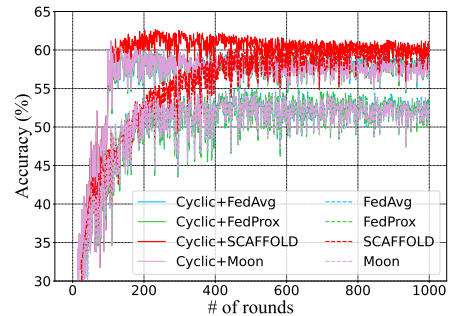


Fig. 3: Test accuracy comparison on CIFAR-10 w/  $\beta = 0.5$ .

TABLE III: Comparison of maximum test accuracy.

Model	Dataset	Non-IID Setting ( $\beta$ )	Accuracy (%) / Rounds					
			FedAvg	FedProx	SCAFFOLD	Moon	Cyclic + FedAvg	
CharLSTM-256	Shakespeare	-	56.35 / 48	46.73 / 50	56.44 / 50	-	<u>57.05 / 49</u>	
CNN-FEMNIST	FEMNIST	-	82.82 / 975	82.82 / 975	83.83 / 995	82.99 / 975	<u>84.62 / 117</u>	
CNN-Fashion-MNIST	Fashion-MNIST	0.1	81.69 / 919	81.52 / 919	82.09 / 761	81.67 / 670	<u>86.19 / 876</u>	
		0.5	86.00 / 911	85.95 / 911	86.25 / 980	86.01 / 936	<u>88.47 / 954</u>	
		1.0	86.58 / 929	86.59 / 837	86.53 / 961	86.31 / 979	<u>88.96 / 860</u>	
LeNet-5	CIFAR-10	0.1	50.77 / 800	50.40 / 800	<u>56.23 / 913</u>	50.51 / 553	54.97 / 787	
		0.5	54.99 / 516	54.99 / 516	<u>61.29 / 781</u>	54.93 / 483	61.08 / <u>107</u>	
		1.0	57.31 / 530	57.60 / 257	<u>63.36 / 762</u>	56.98 / 399	61.45 / <u>129</u>	
ResNet-8	CIFAR-100	Coarse	0.1	44.33 / 591	44.96 / 591	43.50 / 277	44.53 / 591	<u>57.61 / 365</u>
			0.5	56.57 / 934	56.47 / 816	56.15 / 459	56.95 / 955	<u>66.59 / 380</u>
			1.0	58.39 / 977	58.18 / 836	58.96 / 624	58.01 / 858	<u>67.37 / 265</u>
		Fine	0.1	42.83 / 699	42.66 / 836	46.95 / 360	43.17 / 755	<u>56.11 / 252</u>
			0.5	48.86 / 394	48.85 / 683	51.48 / 323	49.21 / 362	<u>58.92 / 150</u>
			1.0	49.88 / 489	50.00 / 607	51.64 / 548	50.18 / 493	<u>58.33 / 128</u>

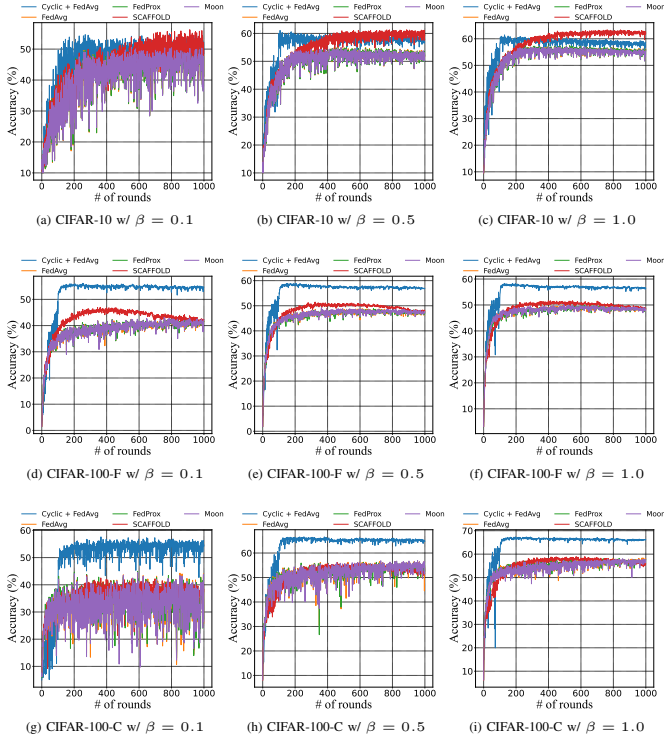


Fig. 4: Test accuracy for CIFAR-10/100.

**Convergence performance.** Table III presents the maximum accuracy and the number of training rounds consumed to achieve it for all baselines. The number of training rounds is underlined for better visualization. We can find that cyclic+fedAvg achieves the highest accuracy in most cases while maintaining the smallest communication rounds consumed. For experiments including CIFAR-10 with  $\beta = 0.5$ , CIFAR-10 with  $\beta = 1.0$ , CIFAR-100-Fine with  $\beta = 0.5$ , and CIFAR-100-Fine with  $\beta = 1.0$ , we can observe a tremendously fast convergence speed when starting training from a cyclic pre-training global model: 7 more rounds are consumed to achieve an accuracy of 61.08%; 29 more rounds to achieve an accuracy of 61.45%; 50 more rounds to achieve 58.92%; and 28 more rounds to achieve 58.33%. For FEMNIST dataset, we can find that it only consumes 17 more rounds to achieve an accuracy of 84.62%. In Figure 4, we showed the learning curves of experiments on CIFAR-10 and CIFAR-100. The

first 100 rounds represent the cyclic training process, and we switched to P2 to complete the rest of the training process (900 rounds). In this figure, we can observe a notable accuracy leap that occurs after switching to P2, which shows the ability of cyclic training to accelerate convergence.

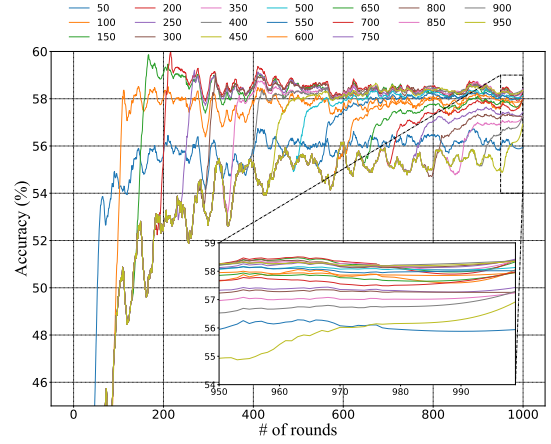


Fig. 5: Learning curves when switching from P1 to P2 at different rounds. The final 50 rounds are zoomed in.

**Impact of cyclic training duration.** Figure 5 compares final test accuracy based on different training rounds spent in P1 while maintaining the maximum local training steps unchanged. The experiments were conducted on CIFAR-10 with  $\beta = 0.5$ , and the total rounds (P1+P2) are 1000. To better visualize the trends of learning curves, all curves are smoothed by the Savitzky-Golay filter [30]. The window size of the filter is 41, and the order is 3. We can observe that the fast convergence phenomenon occurs in all scenarios. Although cyclic training already brings accuracy improvements compared to vanilla FL (e.g., extend cyclic training up to 950 rounds), we can still obtain more improvements in accuracy if we initiate a switching point (e.g., switch to vanilla FL at the 950<sup>th</sup> rounds). Figure 6 shows the relation between the number of training rounds in P1 and the final test accuracy by scatters. We fitted the scatters with a 3<sup>rd</sup> order polynomial curve, which shows the trend of the final accuracy when switching from P1 to P2 at different rounds. Similar to the phenomenon in [23], we can find that the transferability of the pre-trained model rapidly increases at early rounds, followed by a slow descent. Although we can expect more improvements in accuracy if

we increase P1 from 100 rounds to 150 rounds, the advantage of convergence acceleration is diminished due to the extra rounds spent in P1. As a result, a trade-off between efficiency and accuracy performance needs to be considered in practical situations.

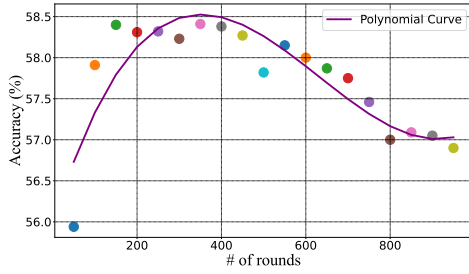


Fig. 6: Test accuracy based on different training rounds in P1.

**Loss landscapes of global models.** Figure 7 visualizes the loss landscapes of models under different Non-IID settings. We conducted experiments on CIFAR-10 with three Non-IID settings using random and pre-trained weights from cyclic training. We projected the trained global models onto their loss landscapes based on the neural network visualization method [19]. The three subfigures on the top describe the loss landscapes of global models from random weights, and the subfigures on the bottom show that from pre-trained weights. We can find that cyclic pre-training results in flatter loss basins and smaller loss values. On the contrary, global models without cyclic pre-training converge to sharp loss basins with larger loss values. We also presented the loss landscapes of the global models obtained from P1 and the randomly initialized global model. Details are presented in Appendix B, where the pre-trained global models show much flatter loss landscapes compared to the randomly initialized one.

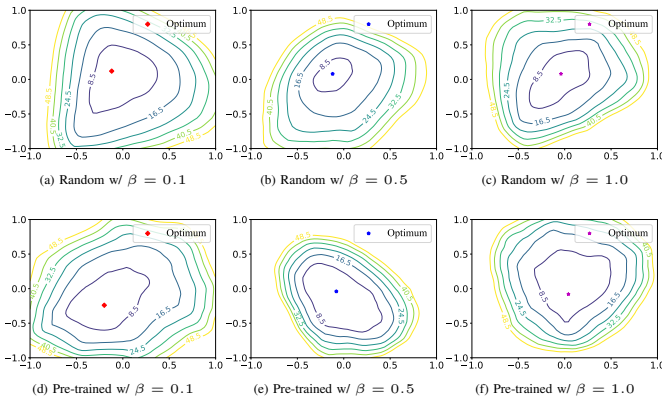


Fig. 7: Loss landscape visualizations of final global models.

**Communication efficiency.** We use notations  $\mathbf{X}$ ,  $T_{cyc}$ ,  $T_{tot}$ ,  $\mathcal{K}_{P1}$ , and  $\mathcal{K}_{P2}$  to represent the capacity of a model, the number of training rounds in P1, the number of training rounds in P2, the number of local clients in P1, and the number of local clients in P2, respectively. We denote  $T_{res} = T_{tot} - T_{cyc}$  to simplify symbols. The overall communication overhead is contributed by training in P1 and P2. In P1, the overhead

is controlled by model transmitting between the cloud server and local clients. Two model transmissions are required in each round, leading to a communication consumption of  $2\mathcal{K}_{P1}\mathbf{X}$  in one training round. Therefore, the overall overhead is  $2\mathcal{K}_{P1}T_{cyc}\mathbf{X}$  in P1. For different FL methods, FedAvg consumes  $2\mathcal{K}_{P2}T_{cyc}\mathbf{X}$ , FedProx and Moon consume the same as FedAvg does. SCAFFOLD demands uploading control variables, thus leading to an overhead of  $4\mathcal{K}_{P2}T_{cyc}\mathbf{X}$  in P1. The communication overhead in P2 depends on which FL algorithm is selected to continue the training procedure. In Table IV, we presented a comprehensive comparison of communication consumption.

TABLE IV: Comparison of communication overhead.

Algorithms	Communication Overhead	
	w/o Cyclic+	w/ Cyclic+
FedAvg	$2\mathcal{K}_{P2}T_{tot}\mathbf{X}$	$2[\mathcal{K}_{P1}T_{cyc} + \mathcal{K}_{P2}T_{res}]\mathbf{X}$
FedProx	$2\mathcal{K}_{P2}T_{tot}\mathbf{X}$	$2[\mathcal{K}_{P1}T_{cyc} + \mathcal{K}_{P2}T_{res}]\mathbf{X}$
Moon	$2\mathcal{K}_{P2}T_{tot}\mathbf{X}$	$2[\mathcal{K}_{P1}T_{cyc} + \mathcal{K}_{P2}T_{res}]\mathbf{X}$
SCAFFOLD	$4\mathcal{K}_{P2}T_{tot}\mathbf{X}$	$2[\mathcal{K}_{P1}T_{cyc} + 2\mathcal{K}_{P2}T_{res}]\mathbf{X}$

## V. CONCLUSION

Although Federated Learning (FL) enables effective knowledge sharing among distributed clients without compromising their data privacy, it suffers from slow convergence and poor classification and prediction performance. To address these issues, this paper presented a novel FL method named CyclicFL, which enables the quick pre-training for effective initial models cyclically on clients rather than public proxy data. Since the pre-trained model can guide the SGD processes during the FL training, the overall FL training process can be accelerated. To theoretically evaluate the performance of CyclicFL, we proved the approximation of CyclicFL to the existing centralized pre-trained methods, and showed the limited Lipschitzness of loss for the pre-trained models by CyclicFL. Comprehensive experimental results show the effectiveness of our proposed CyclicFL.

## REFERENCES

- [1] Mehdi Abbana Bennani, Thang Doan, and Masashi Sugiyama. Generalisation guarantees for continual learning with orthogonal gradient descent. *arXiv preprint arXiv:2006.11942*, 2020.
- [2] Sebastian Caldas, Sai Meher Karthik Duddu, Peter Wu, Tian Li, Jakub Konečný, H Brendan McMahan, Virginia Smith, and Ameet Talwalkar. Leaf: A benchmark for federated settings. *arXiv preprint arXiv:1812.01097*, 2018.
- [3] Hong-You Chen, Cheng-Hao Tu, Ziwei Li, Han-Wei Shen, and Wei-Lun Chao. On pre-training for federated learning. *arXiv preprint arXiv:2206.11488*, 2022.
- [4] Jinyu Chen, Wenchao Xu, Song Guo, Junxiao Wang, Jie Zhang, and Haozhao Wang. Fedtune: A deep dive into efficient federated fine-tuning with pre-trained transformers. *arXiv preprint arXiv:2211.08025*, 2022.
- [5] Jacob Devlin, Ming-Wei Chang, Kenton Lee, and Kristina Toutanova. BERT: Pre-training of deep bidirectional transformers for language understanding. In *Proceedings of the*

- 2019 Conference of the North American Chapter of the Association for Computational Linguistics: Human Language Technologies (ACL), Volume 1 (Long and Short Papers), June 2019.
- [6] Alexey Dosovitskiy, Lucas Beyer, Alexander Kolesnikov, Dirk Weissenborn, Xiaohua Zhai, Thomas Unterthiner, Mostafa Dehghani, Matthias Minderer, Georg Heigold, Sylvain Gelly, Jakob Uszkoreit, and Neil Houlsby. An image is worth 16x16 words: Transformers for image recognition at scale. *International Conference on Machine Learning (ICML)*, 2021.
- [7] Simon S. Du, Xiyu Zhai, Barnabas Poczos, and Aarti Singh. Gradient descent provably optimizes over-parameterized neural networks. In *International Conference on Learning Representations (ICLR)*, 2019.
- [8] Xavier Glorot and Yoshua Bengio. Understanding the difficulty of training deep feedforward neural networks. In *Proceedings of the Thirteenth International Conference on Artificial Intelligence and Statistics (AISTATS)*, pages 249–256. JMLR Workshop and Conference Proceedings, 2010.
- [9] Kaiming He, Xiangyu Zhang, Shaoqing Ren, and Jian Sun. Delving deep into rectifiers: Surpassing human-level performance on imagenet classification. In *Proceedings of the IEEE International Conference on Computer Vision (ICCV)*, pages 1026–1034, 2015.
- [10] Kaiming He, Xiangyu Zhang, Shaoqing Ren, and Jian Sun. Deep residual learning for image recognition. In *Proceedings of the IEEE Conference on Computer Vision and Pattern Recognition (CVPR)*, pages 770–778, 2016.
- [11] Geoffrey Hinton, Oriol Vinyals, Jeff Dean, et al. Distilling the knowledge in a neural network. *arXiv preprint arXiv:1503.02531*, 2(7), 2015.
- [12] Jeremy Howard and Sebastian Ruder. Universal language model fine-tuning for text classification. In *Proceedings of the 56th Annual Meeting of the Association for Computational Linguistics, ACL 2018, Melbourne, Australia, July 15-20, 2018, Volume 1: Long Papers*, pages 328–339, 2018.
- [13] Andrew G Howard, Menglong Zhu, Bo Chen, Dmitry Kalenichenko, Weijun Wang, Tobias Weyand, Marco Andreetto, and Hartwig Adam. Mobilenets: Efficient convolutional neural networks for mobile vision applications. *arXiv preprint arXiv:1704.04861*, 2017.
- [14] Wei Hu, Lechao Xiao, and Jeffrey Pennington. Provable benefit of orthogonal initialization in optimizing deep linear networks. In *International Conference on Learning Representations (ICLR)*, 2020.
- [15] Arthur Jacot, Franck Gabriel, and Clément Hongler. Neural tangent kernel: Convergence and generalization in neural networks. *Advances in Neural Information Processing Systems (NeurIPS)*, 31, 2018.
- [16] Sai Praneeth Karimireddy, Satyen Kale, Mehryar Mohri, Sashank Reddi, Sebastian Stich, and Ananda Theertha Suresh. Scaffold: Stochastic controlled averaging for federated learning. In *International Conference on Machine Learning (ICML)*, pages 5132–5143. PMLR, 2020.
- [17] Alex Krizhevsky, Geoffrey Hinton, et al. Learning multiple layers of features from tiny images. 2009.
- [18] Yann LeCun, Léon Bottou, Yoshua Bengio, and Patrick Haffner. Gradient-based learning applied to document recognition. *Proceedings of the IEEE*, 86(11):2278–2324, 1998.
- [19] Hao Li, Zheng Xu, Gavin Taylor, Christoph Studer, and Tom Goldstein. Visualizing the loss landscape of neural nets. *Advances in Neural Information Processing Systems (NeurIPS)*, 31, 2018.
- [20] Tian Li, Anit Kumar Sahu, Manzil Zaheer, Maziar Sanjabi, Ameet Talwalkar, and Virginia Smith. Federated optimization in heterogeneous networks. *Proceedings of Machine Learning and Systems (MLSys)*, 2:429–450, 2020.
- [21] Qinbin Li, Bingsheng He, and Dawn Song. Model-contrastive federated learning. In *Proceedings of the IEEE/CVF Conference on Computer Vision and Pattern Recognition (CVPR)*, pages 10713–10722, 2021.
- [22] Qinbin Li, Yiqun Diao, Quan Chen, and Bingsheng He. Federated learning on non-iid data silos: An experimental study. In *2022 IEEE 38th International Conference on Data Engineering (ICDE)*, pages 965–978. IEEE, 2022.
- [23] Hong Liu, Mingsheng Long, Jianmin Wang, and Michael I Jordan. Towards understanding the transferability of deep representations. *arXiv preprint arXiv:1909.12031*, 2019.
- [24] Haitao Mao, Xu Chen, Qiang Fu, Lun Du, Shi Han, and Dongmei Zhang. Neuron campaign for initialization guided by information bottleneck theory. In *Proceedings of the 30th ACM International Conference on Information I& Knowledge Management (CIKM)*, page 3328–3332, 2021.
- [25] Brendan McMahan, Eider Moore, Daniel Ramage, Seth Hampson, and Blaise Aguera y Arcas. Communication-efficient learning of deep networks from decentralized data. In *Artificial Intelligence and Statistics (AISTATS)*, pages 1273–1282. PMLR, 2017.
- [26] Vinod Nair and Geoffrey E Hinton. Rectified linear units improve restricted boltzmann machines. In *International Conference on Machine Learning (ICML)*, 2010.
- [27] John Nguyen, Kshitiz Malik, Maziar Sanjabi, and Michael Rabbat. Where to begin? exploring the impact of pre-training and initialization in federated learning. *arXiv preprint arXiv:2206.15387*, 2022.
- [28] Chigozie Nwankpa, Winifred Ijomah, Anthony Gachagan, and Stephen Marshall. Activation functions: Comparison of trends in practice and research for deep learning. *arXiv preprint arXiv:1811.03378*, 2018.
- [29] Alec Radford, Jong Wook Kim, Chris Hallacy, Aditya Ramesh, Gabriel Goh, Sandhini Agarwal, Girish Sastry, Amanda Askell, Pamela Mishkin, Jack Clark, et al. Learning transferable visual models from natural language supervision. In *International Conference on Machine Learning (ICML)*, pages 8748–8763. PMLR, 2021.
- [30] Abraham Savitzky and Marcel JE Golay. Smoothing and differentiation of data by simplified least squares procedures. *Analytical Chemistry*, 36(8):1627–1639, 1964.
- [31] Micah J Sheller, Brandon Edwards, G Anthony Reina,



Jason Martin, Sarthak Pati, Aikaterini Kotrotsou, Mikhail Milchenko, Weilin Xu, Daniel Marcus, Rivka R Colen, et al. Federated learning in medicine: facilitating multi-institutional collaborations without sharing patient data. *Scientific Reports*, 10(1):1–12, 2020.

- [32] Karen Simonyan and Andrew Zisserman. Very deep convolutional networks for large-scale image recognition. *arXiv preprint arXiv:1409.1556*, 2014.
- [33] Jianyu Wang, Qinghua Liu, Hao Liang, Gauri Joshi, and H Vincent Poor. Tackling the objective inconsistency problem in heterogeneous federated optimization. *Advances in neural information processing systems (NeurIPS)*, 33:7611–7623, 2020.
- [34] Han Xiao, Kashif Rasul, and Roland Vollgraf. Fashion-mnist: a novel image dataset for benchmarking machine learning algorithms. *arXiv preprint arXiv:1708.07747*, 2017.
- [35] Wensi Yang, Yuhang Zhang, Kejiang Ye, Li Li, and Cheng-Zhong Xu. Ffd: A federated learning based method for credit card fraud detection. In *International Conference on Big Data*, pages 18–32. Springer, 2019.
- [36] Xinqian Zhang, Ming Hu, Jun Xia, Tongquan Wei, Mingsong Chen, and Shiyan Hu. Efficient federated learning for cloud-based aiot applications. *IEEE Transactions on Computer-Aided Design of Integrated Circuits and Systems*, 40(11):2211–2223, 2021.
- [37] Ligeng Zhu, Zhijian Liu, and Song Han. Deep leakage from gradients. *Advances in Neural Information Processing Systems (NeurIPS)*, 32, 2019.
- [38] Chen Zhu, Renkun Ni, Zheng Xu, Kezhi Kong, W Ronny Huang, and Tom Goldstein. Gradinit: Learning to initialize neural networks for stable and efficient training. *Advances in Neural Information Processing Systems (NeurIPS)*, 34:16410–16422, 2021.
- [39] Hangyu Zhu, Jinjin Xu, Shiqing Liu, and Yaochu Jin. Federated learning on non-iid data: A survey. *Neurocomputing*, 465:371–390, 2021.

## APPENDIX

### A. Derivation of Corollary 1

In this subsection, we show the details of how Corollary 1 is derived from Lemma 1 in [1]. We also explain the intermediate variables in Lemma 1 that compose Corollary 1. In Lemma 1, constant  $n_\tau$  is the number of samples in dataset  $\tau$ . Residual is defined as  $\tilde{y}_\tau = y_\tau - f_{\tau-1}^*(\mathbf{X}_\tau)$  in which  $\mathbf{X}_\tau$  is the data in  $D_\tau$ .  $L_2$  norm coefficient is represented by  $\lambda$ , which is equal to the weight decay. The identity matrix is defined as  $\mathbf{I}$ . The inner product symbol  $\kappa_\tau(\cdot)$  indicates the Neural Tangent Kernel (NTK) [15], which describes the dynamics of training. The NTK is defined as  $\phi_\tau(\mathbf{X})\phi_\tau(\mathbf{X})^T$  where  $\phi_\tau(\mathbf{X}) = \nabla_{\mathbf{w}} f_0^*(\mathbf{X})$ , the gradient of the loss function concerning model parameters  $\mathbf{w}$  at initial state 0. In  $C$ , constant  $c$  evaluates the Lipschitz of the loss function with probability at least  $1 - \delta$ .

Lemma 1 shows empirical losses under three different scenarios when training on a sequence of tasks denoted as

$\tau \in [1, T]$ : OGD for  $\tau \in [1, T]$ , SGD for  $\tau \in [1, T - 1]$  and SGD for  $\tau = T$ . The intermediate variables  $R_T$  and  $H_{k,\tau}$  are shown in the Equations below:

$$R_T = \sum_{\tau=1}^T \sqrt{\frac{\lambda^2 \text{tr}(\kappa_\tau(\mathbf{X}_\tau, \mathbf{X}_\tau))}{n_\tau^2}} R_\lambda, \quad (7)$$

$$H_{k,\tau} = \tilde{\mathbf{y}}_k^\top (\kappa_k(\mathbf{X}_k, \mathbf{X}_k) + \lambda \mathbf{I})^{-1} \cdot \kappa_k(\mathbf{X}_k, \mathbf{X}_\tau) (\kappa_k(\mathbf{X}_k, \mathbf{X}_k) + \lambda \mathbf{I})^{-1} \tilde{\mathbf{y}}_k. \quad (8)$$

To show the difference between OGD-based and SGD-based learning on a continual learning problem through Lemma 1 [1], we analyze it from the perspective of the training loss of optimum model  $f_T^*$  on dataset  $D_\tau$  where  $\tau \leq T$ . For  $\tau = T$ , both OGD and SGD have the same expression, which is composed of two main terms shown in the following equations:

$$\frac{\lambda^2}{n_\tau} \tilde{\mathbf{y}}_\tau^\top (\kappa_\tau(\mathbf{X}_\tau, \mathbf{X}_\tau) + \lambda \mathbf{I})^{-1} \tilde{\mathbf{y}}_\tau, \quad (9)$$

$$\sqrt{\frac{\text{tr}(\kappa_\tau(\mathbf{X}_\tau, \mathbf{X}_\tau))}{n_\tau^2}} \tilde{\mathbf{y}}_\tau^\top (\kappa_\tau(\mathbf{X}_\tau, \mathbf{X}_\tau) + \lambda \mathbf{I})^{-1} \tilde{\mathbf{y}}_\tau. \quad (10)$$

Equation 9 shows that the empirical loss is not zero if a regularization term exists. Equation 10 represents Rademacher Complexity (RC), which quantifies the complexity of a model and decreases as task similarity increases. When  $\tau \leq T$ , the difference based on  $H_{k,\tau}$  lies between the upper bound of OGD-based learning and that of SGD-based learning.  $H_{k,\tau}$  only relates to SGD-based learning and shows the similarity between tasks. Note that the upper bound of SGD is greater than that of OGD. We take an accumulated subtraction to derive the final description:

$$\begin{aligned} \text{Diff} &\triangleq \sum_{\tau=1}^T \mathcal{L}_{D_\tau}^{SGD}(f_T^*) - \mathcal{L}_{D_\tau}^{OGD}(f_T^*) \\ &\leq R_T + \frac{1}{n_T} \sum_{\tau=1}^{T-1} \sum_{k=\tau+1}^T H_{k,\tau}. \end{aligned} \quad (11)$$

### B. Mathematical Notations in Lemma 2

In this subsection, we explain the definitions of  $\lambda_P$  and  $\lambda_Q$  to explain Lemma 2.  $\lambda_P$  and  $\lambda_Q$  are the smallest eigenvalues of  $\mathbf{H}_P^\infty$  and  $\mathbf{H}_Q^\infty$ , respectively.  $\mathbb{I}$  denotes the indicator function. The Gram matrix  $\mathbf{H}_P^\infty$  and  $\mathbf{H}_Q^\infty$  are presented as blew:

$$\begin{aligned} \mathbf{H}_{P,ij}^\infty &= \mathbb{E}_{\mathbf{w} \sim \mathcal{N}(\mathbf{0}, \mathbf{I})} \left[ \mathbf{x}_{P,i}^\top \mathbf{x}_{P,j} \mathbb{I} \left\{ \mathbf{w}^\top \mathbf{x}_{P,i} \geq 0, \mathbf{w}^\top \mathbf{x}_{P,j} \geq 0 \right\} \right] \\ &= \frac{\mathbf{x}_{P,i}^\top \mathbf{x}_{P,j} (\pi - \arccos(\mathbf{x}_{P,i}^\top \mathbf{x}_{P,j}))}{2\pi}, \end{aligned} \quad (12)$$

$$\begin{aligned} \mathbf{H}_{Q,ij}^\infty &= \mathbb{E}_{\mathbf{w} \sim \mathcal{N}(\mathbf{0}, \mathbf{I})} \left[ \mathbf{x}_{Q,i}^\top \mathbf{x}_{Q,j} \mathbb{I} \left\{ \mathbf{w}^\top \mathbf{x}_{Q,i} \geq 0, \mathbf{w}^\top \mathbf{x}_{Q,j} \geq 0 \right\} \right] \\ &= \frac{\mathbf{x}_{Q,i}^\top \mathbf{x}_{Q,j} (\pi - \arccos(\mathbf{x}_{Q,i}^\top \mathbf{x}_{Q,j}))}{2\pi}, \end{aligned} \quad (13)$$

$$\begin{aligned} \mathbf{H}_{PQ,ij}^\infty &= \mathbb{E}_{\mathbf{w} \sim \mathcal{N}(\mathbf{0}, \mathbf{I})} \left[ \mathbf{x}_{P,i}^\top \mathbf{x}_{Q,j} \mathbb{I} \left\{ \mathbf{w}^\top \mathbf{x}_{P,i} \geq 0, \mathbf{w}^\top \mathbf{x}_{Q,j} \geq 0 \right\} \right] \\ &= \frac{\mathbf{x}_{P,i}^\top \mathbf{x}_{Q,j} (\pi - \arccos(\mathbf{x}_{P,i}^\top \mathbf{x}_{Q,j}))}{2\pi}. \end{aligned} \quad (14)$$

$\mathbf{H}_{P,ij}^\infty$  and  $\mathbf{H}_{Q,ij}^\infty$  represent the Gram matrix of input data in dataset P and dataset Q, respectively. Gram matrix  $\mathbf{H}_{PQ,ij}^\infty$  measures the relations between P and Q. Notation  $\mathbf{w}$  is the model parameter, and  $\mathbb{I}$  is the indicator function in Equations 12, 13, and 14. The number of neurons in the given network is defined as  $m$ .  $\mathbf{y}_{P \rightarrow Q}$  is derived from  $(\mathbf{H}_{PQ}^\infty)^T (\mathbf{H}_P^\infty)^{-1} \mathbf{y}_P$ . Coefficient  $\delta$  is the same as what is defined in Lemma 1.

FEMNIST contains 62 classes with 190 clients. Shakespeare includes 660 clients, each owning 5773 data points on average. Fashion-MNIST has 10 classes with 60000 training data and 1000 testing data. CIFAR-10 includes 10 classes, while CIFAR-100 consists of 100 classes. Note that each image in CIFAR-100 is tagged with two types of labels, namely a “fine(F)” label and a “coarse(C)” label. The “fine” label denotes an exact class to which one image belongs, and the “coarse” label represents a superclass to which it belongs. (e.g., A yellow-in-black bee can both belong to an “insect” superclass and to a “bee” exact class). To thoroughly explore the CIFAR-100 dataset, we conducted experiments on “fine” labels and “coarse” labels.

Since our method is accomplished before conventional FL algorithms, we elaborated individual hyperparameters for P1 and P2, respectively. In both phases, we set the total number of clients to 100, except for FEMNIST and Shakespeare. FEMNIST and Shakespeare are naturally Non-IID, the former is attributed to 190 clients, and the latter is split into 660 clients. In P1, we uniformly selected 25% of the total clients to participate in local training in every round by default. The total training rounds in P1 are set to 100 ( $T_{cyc}$ ). The maximum local update steps are set as 20. Note that we set 100 as the maximum local update steps for Shakespeare. In P2, the ratio of clients participating in local training in every round is set as 10%. Note that FedProx and Moon both introduce extra hyperparameters that need to tune. We set the coefficient  $\mu$  in FedProx as 0.01. For Moon, we set the distillation temperature  $T$  as 0.5 and  $\mu$  as 0.1. For vision tasks except for CIFAR-100, we configured the learning rate as 0.01, momentum as 0, and weight decay as 0. For CIFAR-100, the learning rate is 0.1, the momentum to 0.5, and the weight decay is configured as  $1e-3$ . The learning rate decays to its 99.8% after each round. For the language task, the learning rate is set to 1.4, and the momentum and weight decay are set to 0. To make a fair comparison in P2, we set 5 as the number of local epochs for Shakespeare and 5 for others. The training rounds are 50 for Shakespeare and 1000 ( $T_{tot}$ ) for others. For both P1 and P2, we set the batch size to 32.

In this section, all loss landscapes are obtained from experiments on CIFAR-10. Figure 8 shows the loss landscape of the randomly initialized global model. We can observe that the

global model has a sharp loss landscape. Figure 9 shows the loss landscapes of three pre-trained global models on three Non-IID settings: i)  $\beta = 0.1$ ; ii)  $\beta = 0.5$ ; and iii)  $\beta = 1.0$ . Compared to Figure 8, every pre-trained global has a flatter loss landscape.

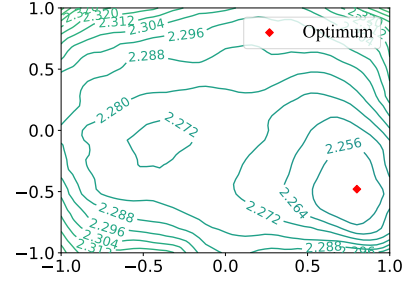


Fig. 8: Visualizations of loss landscapes of the randomly initialized global model.

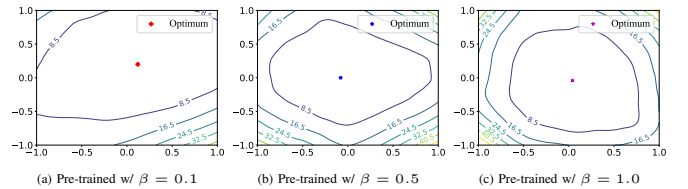


Fig. 9: Visualizations of loss landscapes of the pre-trained global model on different Non-IID scenarios.